PENETRATION OF MICROWAVES THROUGH DISPERSIVE CONCRETE USING A THREE-DIMENSIONAL FINITE-DIFFERENCE TIME-DOMAIN CODE

S. Joe Yakura and David Dietz

30 June 1999

Final Report

19990909 111

APPROVED FOR PUBLIC RELEASE; DISTRIBUTION IS UNLIMITED.

AIR FORCE RESEARCH LABORATORY
Directed Energy Directorate
3550 Aberdeen Ave SE
AIR FORCE MATERIEL COMMAND
KIRTLAND AIR FORCE BASE, NM 87117-5776

DTIC QUALITY INSPECTED 4

AFRL-DE-TR-1999-1054

This report has been approved for publication.

S. JOE YAKURA, DR-III, (GS-14)
Project Manager

FOR THE COMMANDER

JORGE E. BERAUN, DR-IV, (GS-15)   R. EARL GOOD, SES
Chief, Branch   Director, Directed Energy

REPORT DOCUMENTATION PAGE

Form Approved
OMB No. 074-0188

Public reporting burden for this collection of information is estimated to average 1 hour per response, including the time for reviewing instructions, searching existing data sources, gathering and maintaining the data needed, and completing and reviewing this collection of information. Send comments regarding this burden estimate or any other aspect of this collection of information, including suggestions for reducing this burden to Washington Headquarters Services, Directorate for Information Operations and Reports, 1215 Jefferson Davis Highway, Suite 1204, Arlington, VA 22202-4302, and to the Office of Management and Budget, Paperwork Reduction Project (0704-0188), Washington, DC 20503

1. AGENCY USE ONLY (Leave blank)	2. REPORT DATE 30 June 1999	3. REPORT TYPE AND DATES COVERED Final; 1 January 1999 – 30 June 1999

4. TITLE AND SUBTITLE
Penetration of Microwaves Through Dispersive Concrete
Using a Three-Dimensional Finite-Difference Time-Domain Code

5. FUNDING NUMBERS
PE: 62601F
PR: 5797
TA: AL

WW:03

6. AUTHOR(S)
S. Joe Yakura and David Dietz

7. PERFORMING ORGANIZATION NAME(S) AND ADDRESS(ES)

Air Force Research Laboratory
Directed Energy Directorate
(AFRL/DEPE)
3550 Aberdeen Ave SE
Kirtland Air Force Base, NM 87117-5776

8. PERFORMING ORGANIZATION REPORT NUMBER

AFRL-DE-TR-1999-1054

9. SPONSORING / MONITORING AGENCY NAME(S) AND ADDRESS(ES)

10. SPONSORING / MONITORING AGENCY REPORT NUMBER

11. SUPPLEMENTARY NOTES

12a. DISTRIBUTION / AVAILABILITY STATEMENT
Approved for public release; distribution is unlimited.

12b. DISTRIBUTION CODE

13. ABSTRACT (Maximum 200 Words)
In this paper, we present a new formulation of a three-dimensional Finite-Difference Time-Domain (FDTD) algorithm that is applicable for studying the penetration of microwave pulses in conductive and dispersive materials, such as concrete. We investigate the effects of microwaves penetrating into conductive and dispersive concrete using the newly formulated algorithm incorporated into a three-dimensional FDTD code. Because of the dispersive properties of concrete, both conductivity and polarization are taken to be frequency-dependent. We model the electric polarization terms and the electric conductivity to exhibit linear dispersive behavior via first-order, time-dependent, electric susceptibility and conductivity functions. Sample one-dimensional FDTD calculations show that the penetration of wide-band and ultrawide-band microwave pulses must be simulated using the fully dispersive FDTD algorithm to obtain the proper response from dispersive concrete. On the other hand, the use of the fully dispersive FDTD algorithm is not essential in simulating the penetration of narrow-band microwave pulses through concrete because of the non-dispersive nature of the narrow-band (single frequency) effect.

14. SUBJECT TERMS
Computational Electromagnetics, Numerical Analysis

15. NUMBER OF PAGES
28

16. PRICE CODE

17. SECURITY CLASSIFICATION OF REPORT unclassified	18. SECURITY CLASSIFICATION OF THIS PAGE unclassified	19. SECURITY CLASSIFICATION OF ABSTRACT unclassified	20. LIMITATION OF ABSTRACT Unlimited

NSN 7540-01-280-5500

Standard Form 298 (Rev. 2-89)
Prescribed by ANSI Std. Z39-18
298-102

TABLE OF CONTENTS

LIST OF FIGURES

Penetration of Microwaves Through Dispersive Concrete Using a Three-Dimensional Finite-Difference Time-Domain Code

S. J. Yakura and D. Dietz
Air Force Research Laboratory, Directed Energy Directorate
Kirtland AFB, NM 87117-5776

Abstract

In this paper, we present a new formulation of a three-dimensional Finite-Difference Time-Domain (FDTD) algorithm that is applicable for studying the penetration of microwave pulses in conductive and dispersive materials, such as concrete. We investigate the effects of microwaves penetrating into conductive and dispersive concrete using the newly formulated algorithm incorporated into a three-dimensional FDTD code. Because of the dispersive properties of concrete, both conductivity and polarization terms are taken to be frequency-dependent. We model the electric polarization terms and the electric conductivity to exhibit linear dispersive behavior via first-order, time-dependent, electric susceptibility and conductivity functions. Sample one-dimensional FDTD calculations show that the penetration of wide-band and ultrawide-band microwave pulses must be simulated using the fully dispersive FDTD algorithm to obtain the proper response from dispersive concrete. On the other hand, the use of the fully dispersive FDTD algorithm is not essential in simulating the penetration of narrow-band microwave pulses through concrete because of the non-dispersive nature of the narrow-band (single frequency) effect.

I. INTRODUCTION

Determining the penetration through concrete of microwaves using numerical modeling has received much attention in recent years. Measured ground penetration radar data in the range of 600 MHz to 3 GHz has shown concrete to exhibit dispersive characteristics in both electrical permittivity and conductivity. Based on the experimental data now available from many experiments that have been carried out in last few years, we have sufficient information to simulate the detailed behavior of microwave pulses that penetrate through dispersive concrete materials [1-3].

With the advent of present day computers which provide very fast execution times and great quantities of computer memory, we are at the point where we have enough computational power to solve Maxwell's equations directly for a large-scale problem. Among recently investigated numerical techniques that show great promise in achieving this goal is the well-known finite-difference time-domain (FDTD) method [4]. It is based on using a simple differencing scheme in both time and space to calculate the transient behavior of electromagnetic field quantities. Because of the simplicity of the FDTD method, recent researchers have focused their attention on the numerical evaluation of the linear convolution integral terms which appear in one of Maxwell's equations (Ampère's Law). By properly evaluating these terms, many people have successfully modeled the response of linear dispersive effects [5-10].

In this paper we consider the dispersive materials that exhibit the linear polarization through the first-order, time-dependent, electric susceptibility function. For such materials the relationship between $\underline{D}(t;\underline{x})$ and $\underline{E}(t;\underline{x})$ can be expressed as [11]

$$\underline{D}(t;\underline{x}) = \epsilon_o \epsilon_\infty \underline{E}(t;\underline{x}) + \epsilon_o \sum_{p=1}^{p_{max}} \int_{-\infty}^{\infty} \underline{E}(\tau;\underline{x}) X_p^{(1)}(t-\tau) d\tau, \qquad (1.1)$$

where ϵ_o is the electric permittivity of free space, ϵ_∞ is the medium permittivity at infinite frequency, and $X_p^{(1)}(t-\tau)$ is the pth term of the collection consisting of p_{max} first-order, time-dependent, electric susceptibility functions, where p_{max} is the maximum number of terms which we choose to consider for a particular formulation of Eq. (1.1).

Also, we consider that the current density vector, $\underline{J}(t;\underline{x})$, which appears in one of Maxwell's equations (Ampere's Law), to be dispersive. To include the dispersive characteristics of the current density vector, we first divided the current density vector into non-dispersive and dispersive terms. The non-dispersive term is expressed in the usual form as the product of the constant conductivity coefficient and the electric field vector, $E(t,x)$. The dispersive term is expressed in the linear convolution integral of $\underline{E}(t;\underline{x})$ and the first-order time-dependent conductivity function. Hence, the expression that represents the current density vector, $\underline{J}(t;\underline{x})$, is given in the following form:

$$\underline{J}(t;\underline{x}) = \underline{E}(t;\underline{x}) \sum_{\kappa=1}^{\kappa_{max}} \sigma_\kappa^{(0)} + \sum_{\kappa=1}^{\kappa_{max}} \int_{-\infty}^{\infty} \underline{E}(\tau;\underline{x}) \sigma_\kappa^{(1)}(t-\tau) d\tau, \qquad (1.2)$$

1

where $\sigma_\kappa^{(0)}$ and $\sigma_\kappa^{(1)}(t\text{-}\tau)$ are the κth terms of the collection consisting, respectively, of κ_{max} constant conductivity values and κ_{max} first-order, time-dependent, conductivity functions, where κ_{max} is the maximum number of terms which we choose to consider for a particular formulation of Eq. (1.2).

By including the dispersive contributions in both polarization and current density vectors as shown in Eqs. (1.1) and (1.2), we can evaluate the linear convolution integrals that appear in Maxwell's equations (Ampere's Law) and come up with a second order accurate FDTD algorithm to simulate the characteristic behavior of a wave propagating into a linear dispersive material. We investigate, in particular, the case in which the first-order, time-dependent, electric susceptibility and conductivity functions are expressed in the following complex exponential forms that contain complex constant coefficients:

$$X_\rho^{(1)}(t) = Re\{\alpha_\rho^L exp(-\gamma_\rho^L t)\} U(t),$$

(1.3)

and

$$\sigma_\kappa^{(1)}(t) = Re\{\beta_\kappa^L exp(-\theta_\kappa^L t)\} U(t).$$

(1.4)

where $Re\{\}$ is used to represent the real part of a complex function, $U(t)$ is the unit step function, and α_ρ^L, β_κ^L, γ_ρ^L, and θ_κ^L are complex constant coefficients; superscript L is used to denote the linear coefficient. By making the proper choices of complex constant coefficients and performing Fourier transforms, we can readily obtain the familiar Debye and Lorentz forms of the complex conductivity and permittivity in the frequency domain. [11]

By making use of the our newly formulated three-dimensional FDTD algorithm introduced in this paper, we investigate much needed information about the extent of penetration of microwaves into concrete for various types of externally applied incident pulses. We discuss the results of numerical simulations of high-power microwaves penetrating into concrete that is identified by frequency-dependent conductivity and permittivity. The resulting FDTD calculations provide second order accuracy in both space and time and use the memory-efficient recursive-convolution (RC) technique to update electromagnetic-field quantities. We present in this paper the results that show the distinct difference in the penetration of the wide-band pulse as compared to the narrow-band pulse due to the dispersive nature of concrete.

II. FDTD FORMULATION

In light of Eqs. (1.1) and (1.2), we write Maxwell's equations inside the dispersive material as

$$\frac{\partial[\mu H(t;\underline{x})]}{\partial t} = -\underline{\nabla} \times \underline{E}(t;\underline{x}),$$

(2.1)

$$\frac{\partial \underline{D}(t;\underline{x})}{\partial t} = \underline{\nabla} \times \underline{H}(t;\underline{x}) - \underline{E}(t;\underline{x}) \sum_\kappa \sigma_\kappa^{(0)} - \sum_\kappa \underline{J}_\kappa^L(t;\underline{x}),$$

(2.2)

with

$$\underline{D}(t;\underline{x}) = \epsilon_o \epsilon_\infty \underline{E}(t;\underline{x}) + \epsilon_o \sum_\rho \underline{P}_\rho^L(t;\underline{x}),$$

(2.3)

$$\underline{P}_\rho^L(t;\underline{x}) \equiv \int_{-\infty}^{\infty} \underline{E}(\tau;\underline{x}) X_\rho^{(1)}(t-\tau) d\tau,$$

(2.4)

$$\underline{J}_\kappa^L(t;\underline{x}) \equiv \int_{-\infty}^{\infty} \underline{E}(\tau;\underline{x}) \sigma_\kappa^{(1)}(t-\tau) d\tau,$$

(2.5)

where $\underline{H}(t;\underline{x})$ is the magnetic field vector, μ is the magnetic permeability, $\underline{P}_\rho^L(t;\underline{x})$ is related to the ρth terms of the linear polarization field vector, and $\underline{J}_\kappa^L(t;\underline{x})$ is the first-order time-dependent conductivity. Using an FDTD algorithm, the above equations can be solved numerically at each time step provided we know how to handle $\underline{J}_\kappa^L(t;\underline{x})$ and $\underline{P}_\rho^L(t;\underline{x})$ numerically. Therefore, the whole solution rests on the question of how to carry out the numerical evaluation of $\underline{J}_\kappa^L(t;\underline{x})$ and $\underline{P}_\rho^L(t;\underline{x})$ at each successive time step. For that reason, the rest of this section is devoted to the discussion of numerical formulation that treats $\underline{J}_\kappa^L(t;\underline{x})$ and $\underline{P}_\rho^L(t;\underline{x})$.

2

To obtain second-order accuracy in time in evaluating the convolution integrals, $\underline{E}(t;\underline{x})$ is approximated by a piecewise continuous function over the entire temporal integration range so that $\underline{E}(t;\underline{x})$ changes linearly with respect to time over a given discrete time interval $[m\Delta t, (m+1)\Delta t]$, where $m=0,1,...,n$, with $n\Delta t$ being the current time step [12-14]. Thus, the mathematical expression for $\underline{E}(t;\underline{x})$ takes the following form which can be expressed in terms of the electric field values, $\underline{E}_{ijk}^{m}$ and $\underline{E}_{ijk}^{m+1}$, respectively, evaluated at discrete time steps $t=m\Delta t$ and $t=(m+1)\Delta t$ where these two successive times are obtained at the same discrete spatial location $\underline{x}=(i\Delta x, j\Delta y, k\Delta z)$ with Δx, Δy and Δz being the spatial grid sizes in the x, y and z directions, respectively (we use a superscript to designate the discrete time step and a subscript for the discrete spatial location):

$$\underline{E}(t;\underline{x})_{\underline{x}=(i\Delta x, j\Delta y, k\Delta z)} = \begin{cases} \underline{E}_{ijk}^{m} + \dfrac{(\underline{E}_{ijk}^{m+1} - \underline{E}_{ijk}^{m})}{\Delta t}(t - m\Delta t), & \text{for } 0 \le m\Delta t \le t \le (m+1)\Delta t \le (n+1)\Delta t \\ 0, & \text{for } t \le 0 \end{cases} \quad (2.6)$$

For three-dimensional FDTD calculations in Cartesian coordinates, we need to solve the following discrete forms of Maxwell's equations that obtained from Eqs. (2.1) and (2.2) by finite differencing in both time and space using the usual Yee algorithm [4]:

$$\mu(H_{ijk}^{n+\frac{1}{2}})_x - \mu(H_{ijk}^{n-\frac{1}{2}})_x = \left\{ \frac{\Delta t}{\Delta z} [(E_{ij(k+\frac{1}{2})}^{n})_y - (E_{ij(k-\frac{1}{2})}^{n})_y] - \frac{\Delta t}{\Delta y} [(E_{i(j+\frac{1}{2})k}^{n})_z - (E_{i(j-\frac{1}{2})k}^{n})_z] \right\}, \quad (2.7)$$

$$\mu(H_{ijk}^{n+\frac{1}{2}})_y - \mu(H_{ijk}^{n-\frac{1}{2}})_y = \left\{ \frac{\Delta t}{\Delta x} [(E_{(i+\frac{1}{2})jk}^{n})_z - (E_{(i-\frac{1}{2})jk}^{n})_z] - \frac{\Delta t}{\Delta z} [(E_{ij(k+\frac{1}{2})}^{n})_x - (E_{ij(k-\frac{1}{2})}^{n})_x] \right\}, \quad (2.8)$$

$$\mu(H_{ijk}^{n+\frac{1}{2}})_z - \mu(H_{ijk}^{n-\frac{1}{2}})_z = \left\{ \frac{\Delta t}{\Delta y} [(E_{i(j+\frac{1}{2})k}^{n})_x - (E_{i(j-\frac{1}{2})k}^{n})_x] - \frac{\Delta t}{\Delta x} [(E_{(i+\frac{1}{2})jk}^{n})_y - (E_{(i-\frac{1}{2})jk}^{n})_y] \right\}, \quad (2.9)$$

$$(D_{ijk}^{n+1})_x - (D_{ijk}^{n})_x = \left\{ \frac{\Delta t}{\Delta y} [(H_{i(j+\frac{1}{2})k}^{n+\frac{1}{2}})_z - (H_{i(j-\frac{1}{2})k}^{n+\frac{1}{2}})_z] - \frac{\Delta t}{\Delta z} [(H_{ij(k+\frac{1}{2})}^{n+\frac{1}{2}})_y - (H_{ij(k-\frac{1}{2})}^{n+\frac{1}{2}})_y] \right\}$$

$$- \left\{ \int_{n\Delta t}^{(n+1)\Delta t} (E(t;\underline{x})_{\underline{x}=(i\Delta x, j\Delta y, k\Delta z)})_x \, dt \sum_{\kappa} \sigma_{\kappa}^{(0)} \right\} - \left\{ \sum_{\kappa} \int_{n\Delta t}^{(n+1)\Delta t} (J_{\kappa}^{L}(t;\underline{x})_{\underline{x}=(i\Delta x, j\Delta y, k\Delta z)})_x \, dt \right\}, \quad (2.10)$$

$$(D_{ijk}^{n+1})_y - (D_{ijk}^{n})_y = \left\{ \frac{\Delta t}{\Delta z} [(H_{ij(k+\frac{1}{2})}^{n+\frac{1}{2}})_x - (H_{ij(k-\frac{1}{2})}^{n+\frac{1}{2}})_x] - \frac{\Delta t}{\Delta x} [(H_{(i+\frac{1}{2})jk}^{n+\frac{1}{2}})_z - (H_{(i-\frac{1}{2})jk}^{n+\frac{1}{2}})_z] \right\}$$

$$- \left\{ \int_{n\Delta t}^{(n+1)\Delta t} (E(t;\underline{x})_{\underline{x}=(i\Delta x, j\Delta y, k\Delta z)})_y \, dt \sum_{\kappa} \sigma_{\kappa}^{(0)} \right\} - \left\{ \sum_{\kappa} \int_{n\Delta t}^{(n+1)\Delta t} (J_{\kappa}^{L}(t;\underline{x})_{\underline{x}=(i\Delta x, j\Delta y, k\Delta z)})_y \, dt \right\}, \quad (2.11)$$

$$(D_{ijk}^{n+1})_z - (D_{ijk}^{n})_z = \left\{ \frac{\Delta t}{\Delta x} [(H_{(i+\frac{1}{2})jk}^{n+\frac{1}{2}})_y - (H_{(i-\frac{1}{2})jk}^{n+\frac{1}{2}})_y] - \frac{\Delta t}{\Delta y} [(H_{i(j+\frac{1}{2})k}^{n+\frac{1}{2}})_x - (H_{i(j-\frac{1}{2})k}^{n+\frac{1}{2}})_x] \right\}$$

$$- \left\{ \int_{n\Delta t}^{(n+1)\Delta t} (E(t;\underline{x})_{\underline{x}=(i\Delta x, j\Delta y, k\Delta z)})_z \, dt \sum_{\kappa} \sigma_{\kappa}^{(0)} \right\} - \left\{ \sum_{\kappa} \int_{n\Delta t}^{(n+1)\Delta t} (J_{\kappa}^{L}(t;\underline{x})_{\underline{x}=(i\Delta x, j\Delta y, k\Delta z)})_z \, dt \right\}. \quad (2.12)$$

To evaluate the right-hand side of Eqs. (2.10-2.12), we first begin by substituting Eq. (1.3) into Eq. (2.4) then differentiating these integrals with respect to time to obtain the following first-order differential equation for complex function $Q_{\rho}^{L}(t;\underline{x})$ [14]:

$$\frac{\partial \underline{Q}_{\rho}^{L}(t;\underline{x})}{\partial t} + \gamma_{\rho}^{L} \underline{Q}_{\rho}^{L}(t;\underline{x}) = \alpha_{\rho}^{L} \underline{E}(t;\underline{x}). \quad (2.13)$$

From the above equation, the linear polarization vector, $\underline{P}_{\rho}^{L}(t;\underline{x})$, can be obtained simply by taking the real part of $Q_{\rho}^{L}(t;\underline{x})$. Now, solving the equation *exactly* in time by using the integrating factor, $exp(\gamma_{\rho}^{L} t)$, and then performing the time integration from $n\Delta t$ to $(n+1)\Delta t$, we have

3

$$\underline{Q}_\rho^L(n\Delta t + \Delta t; \underline{x}) = exp(-\gamma_\rho^L \Delta t)\underline{Q}_\rho^L(n\Delta t; \underline{x}) + \alpha_\rho^L exp(-\gamma_\rho^L \Delta t)\int_{n\Delta t}^{n\Delta t + \Delta t}\underline{E}(\tau;\underline{x})exp[-\gamma_\rho^L(n\Delta t - \tau)]d\tau. \qquad (2.14)$$

Based on the piecewise linear approximation which we have considered for the temporal behavior of $\underline{E}(t;\underline{x})$, we can substitute Eq. (2.6) into the right-hand side (i.e., the inhomogeneous part) of Eq. (2.14) for $\underline{E}(\tau;\underline{x})$. Evaluating at spatial location $\underline{x}=(i\Delta x,j\Delta y,k\Delta z)$, these equations result in the following recursive relationship for $(Q_\rho^L)_{ijk}^{n+1}$ in terms of $(Q_\rho^L)_{ijk}^n$, $\underline{E}_{ijk}^n$ and $\underline{E}_{ijk}^{n+1}$:

$$\underline{Q}_\rho^L(n\Delta t + \Delta t; i\Delta x, j\Delta y, k\Delta z) \equiv (\underline{Q}_\rho^L)_{ijk}^{n+1} = exp(-\gamma_\rho^L \Delta t)(\underline{Q}_\rho^L)_{ijk}^n + \underline{E}_{ijk}^n(\psi_{\rho,0}^L) + (\underline{E}_{ijk}^{n+1} - \underline{E}_{ijk}^n)(\psi_{\rho,1}^L), \qquad (2.15)$$

where

$$(\psi_{\rho,0}^L) \equiv \alpha_\rho^L \int_{n\Delta t}^{(n+1)\Delta t} exp[-\gamma_\rho^L(n\Delta t + \Delta t - \tau)]d\tau = \alpha_\rho^L \int_0^{\Delta t} exp(-\gamma_\rho^L \tau)d\tau = \frac{\alpha_\rho^L}{\gamma_\rho^L}[1 - exp(-\gamma_\rho^L \Delta t)], \qquad (2.16)$$

$$(\psi_{\rho,1}^L) \equiv \frac{\alpha_\rho^L}{\Delta t}\int_0^{\Delta t}(\Delta t - \tau)exp(-\gamma_\rho^L \tau)d\tau = \frac{\alpha_\rho^L}{\gamma_\rho^L}\{1 - \frac{1}{\gamma_\rho^L \Delta t}[1 - exp(-\gamma_\rho^L \Delta t)]\}. \qquad (2.17)$$

When Eqs. (2.15) is used in Eq. (2.3) to obtain discrete forms of Eq. (2.3) at successive times $t=n\Delta t$ and $t=(n+1)\Delta t$ and at specific spatial location $\underline{x}=(i\Delta x,j\Delta y,k\Delta z)$, we can express $\underline{D}_{ijk}^n$ and $\underline{D}_{ijk}^{n+1}$, respectively, in the following forms:

$$\underline{D}_{ijk}^n = \epsilon_o \epsilon_\infty \underline{E}_{ijk}^n + \epsilon_o Re\{\sum_\rho (\underline{Q}_\rho^L)_{ijk}^n\}, \qquad (2.18)$$

and

$$\underline{D}_{ijk}^{n+1} = \epsilon_o \epsilon_\infty \underline{E}_{ijk}^{n+1} + \epsilon_o Re\{\sum_\rho [exp(-\gamma_\rho^L \Delta t)][(\underline{Q}_\rho^L)_{ijk}^n] + \underline{E}_{ijk}^n(\psi_{\rho,0}^L) + (\underline{E}_{ijk}^{n+1} - \underline{E}_{ijk}^n)(\psi_{\rho,1}^L)]\}. \qquad (2.19)$$

Subtracting Eq. (2.18) from Eq. (2.19), we obtain the following expression for the left-hand side of Eqs. (2.10-2.12) in terms of $(Q_\rho^L)_{ijk}^n$, $\underline{E}_{ijk}^n$ and $\underline{E}_{ijk}^{n+1}$:

$$\underline{D}_{ijk}^{n+1} - \underline{D}_{ijk}^n = \epsilon_o \epsilon_\infty(\underline{E}_{ijk}^{n+1} - \underline{E}_{ijk}^n)$$
$$+ \epsilon_o Re\{\sum_\rho [[exp(-\gamma_\rho^L \Delta t) - 1][(\underline{Q}_\rho^L)_{ijk}^n] + \underline{E}_{ijk}^n(\psi_{\rho,0}^L) + (\underline{E}_{ijk}^{n+1} - \underline{E}_{ijk}^n)(\psi_{\rho,1}^L)]\}. \qquad (2.20)$$

To evaluate the second term of the right-hand side of Eqs. (2.10-2.12), we substitute Eq. (2.6) for $\underline{E}(t;\underline{x})_{\underline{x}=(i\Delta x,j\Delta y,k\Delta z)}$ and obtain the following expression:

$$\{\int_{n\Delta t}^{(n+1)\Delta t}\underline{E}(t;\underline{x})_{\underline{x}=(i\Delta x,j\Delta y,k\Delta z)}\,dt\sum_\kappa \sigma_\kappa^{(0)}\} = \frac{\Delta t}{2}(\underline{E}_{ijk}^{n+1} + \underline{E}_{ijk}^n)\sum_\kappa \sigma_\kappa^{(0)}. \qquad (2.21)$$

To evaluate the third term of the right-hand side of Eqs. (2.11-2.13), we first substitute Eq. (1.4) into Eq. (2.5) and then differentiate the integral with respect to time to obtain the following first-order differential equation for complex function $\underline{J}_\kappa^L(t;\underline{x})$:

$$\frac{\partial \underline{J}_\kappa^L(t;\underline{x})}{\partial t} + \theta^L \underline{J}_\kappa^L(t;\underline{x}) = \beta_\kappa^L \underline{E}(t;\underline{x}). \qquad (2.22)$$

As in the case of the linear polarization vector, the current density vector, $\underline{J}_\kappa^L(t;\underline{x})$, can be obtained simply by taking the real part of $\underline{J}_\kappa^L(t;\underline{x})$ as seen in the above equation. Once again, we solve the above differential equation *exactly*

by using integrating factor $exp(\theta^L t)$ and then performing the time integration from $n\Delta t$ to t to get the following expression for complex function $\underline{J}_\kappa^L(t;\underline{x})$:

$$\underline{J}_\kappa^L(t;\underline{x}) = exp[\theta_\kappa^L(n\Delta t - t)]\underline{J}_\kappa^L(n\Delta t;\underline{x}) + \beta_\kappa^L exp(-\theta_\kappa^L t)\int_{n\Delta t}^t exp(\theta_\kappa^L \tau)\underline{E}(\tau;\underline{x})d\tau .$$ (2.23)

Again, we substitute Eq. (2.6) into the above equation for $\underline{E}(\tau;\underline{x})$ based on the piecewise linear approximation. Then we integrate Eq. (2.23) from $n\Delta t$ to $n\Delta t + \Delta t$, evaluated at spatial location $\underline{x}=(i\Delta x, j\Delta y, k\Delta z)$, to obtain the following expression for the third term of the right-hand side of Eqs. (2.10-2.12):

$$\int_{n\Delta t}^{(n+1)\Delta t} \underline{J}_\kappa^L(t;\underline{x})_{\underline{x}=(i\Delta x, j\Delta y, k\Delta z)} dt = Re\{ \int_{n\Delta t}^{(n+1)\Delta t} \underline{J}_\kappa^L(t;\underline{x})_{\underline{x}=(i\Delta x, j\Delta y, k\Delta z)} dt \}$$

$$= Re\{ exp(\theta_\kappa^L n\Delta t)\underline{J}_\kappa^L(n\Delta t; i\Delta x, j\Delta y, k\Delta z) \int_{n\Delta t}^{(n+1)\Delta t} exp(-\theta_\kappa^L t)dt$$

$$+ \beta_\kappa^L \int_{n\Delta t}^{(n+1)\Delta t} dt \int_{n\Delta t}^t exp[\theta_\kappa^L(\tau - t)]\underline{E}(\tau;\underline{x})_{\underline{x}=(i\Delta x, j\Delta y, k\Delta z)} d\tau \}$$

$$= Re\{ exp(\theta_\kappa^L n\Delta t)(\underline{J}_\kappa^L)_{ijk}^n \int_{n\Delta t}^{(n+1)\Delta t} exp(-\theta_\kappa^L t)dt$$

$$+ \beta_\kappa^L \int_{n\Delta t}^{(n+1)\Delta t} dt \int_{n\Delta t}^t exp[\theta_\kappa^L(\tau - t)][\underline{E}_{ijk}^n + \frac{(\underline{E}_{ijk}^{n+1} - \underline{E}_{ijk}^n)}{\Delta t}(\tau - n\Delta t)] d\tau \}$$

$$= Re\{ \frac{1}{\theta_\kappa^L}[1 - exp(-\theta_\kappa^L \Delta t)](\underline{J}_\kappa^L)_{ijk}^n + \underline{E}_{ijk}^n(\xi_{\kappa,0}^L) + (\underline{E}_{ijk}^{n+1} - \underline{E}_{ijk}^n)(\xi_{\kappa,1}^L) \},$$ (2.24)

where

$$(\xi_{\kappa,0}^L) \equiv \beta_\kappa^L \int_{n\Delta t}^{(n+1)\Delta t} dt \int_{n\Delta t}^t exp[\theta_\kappa^L(\tau - t)]d\tau = \frac{\beta_\kappa^L \Delta t}{\theta_\kappa^L}\{ 1 - \frac{1}{\theta_\kappa^L \Delta t}[1 - exp(-\theta_\kappa^L \Delta t)]\},$$ (2.25)

$$(\xi_{\kappa,1}^L) \equiv \frac{\beta_\kappa^L}{\Delta t} \int_{n\Delta t}^{(n+1)\Delta t} dt \int_{n\Delta t}^t (\tau - n\Delta t)exp[\theta_\kappa^L(\tau - t)]d\tau = \frac{\beta_\kappa^L \Delta t}{\theta_\kappa^L}\{ \frac{1}{2} - \frac{1}{\theta_\kappa^L \Delta t} + \frac{1}{(\theta_\kappa^L \Delta t)^2}[1 - exp(-\theta_\kappa^L \Delta t)]\}.$$ (2.26)

The expression for $(\underline{J}_\kappa^L)_{ijk}^n$, which appears in Eq. (2.24), can be obtained in the recursive form when we solve Eq. (2.22) *exactly* for $\underline{J}_\kappa^L(t;\underline{x})$ using integrating factor $exp(\theta^L t)$ and then performing the time integration from $t=(n-1)\Delta t$ to $t=n\Delta t$ while making use of the piecewise linear approximation for $\underline{E}(t;\underline{x})$ to evaluate the integral in the right-hand side of Eq. (2.22). The result is that we obtain the following recursive relationship for $(\underline{J}_\kappa^L)_{ijk}^n$ which is expressed in terms of $(\underline{J}_\kappa^L)_{ijk}^{n-1}$, $\underline{E}_{ijk}^{n-1}$ and $\underline{E}_{ijk}$:

$$(\underline{J}_\kappa^L)_{ijk}^n = exp(-\theta_\kappa^L \Delta t)(\underline{J}_\kappa^L)_{ijk}^{n-1} + \underline{E}_{ijk}^{n-1}(\zeta_{\kappa,0}^L) + (\underline{E}_{ijk}^n - \underline{E}_{ijk}^{n-1})(\zeta_{\kappa,1}^L) \},$$ (2.27)

where

$$(\zeta_{\kappa,0}^L) \equiv \beta_\kappa^L \int_{(n-1)\Delta t}^{n\Delta t} exp[-\theta_\kappa^L(n\Delta t - \tau)] d\tau = \beta_\kappa^L \int_0^{\Delta t} exp(-\theta_\kappa^L \tau')d\tau' = \frac{\beta_\kappa^L}{\theta_\kappa^L}[1 - exp(-\theta_\kappa^L \Delta t)],$$ (2.28)

$$(\zeta_{\kappa,1}^L) \equiv \frac{\beta_\kappa^L}{\Delta t} \int_0^{\Delta t}(\Delta t - \tau')exp(-\theta_\kappa^L \tau')d\tau' = \frac{\beta_\kappa^L}{\theta_\kappa^L}\{ 1 - \frac{1}{\theta_\kappa^L \Delta t}[1 - exp(-\theta_\kappa^L \Delta t)]\}.$$ (2.29)

5

Finally, when Eqs. (2.20), (2.21) and (2.24) are substituted into Eqs. (2.10-2.12), we obtain the following expressions for $(E_{ijk}^{n+1})_x$, $(E_{ijk}^{n+1})_y$ and $(E_{ijk}^{n+1})_z$ in terms of known quantities $(Q_\rho^L)_{ijk}^n$, $(\underline{J}_\kappa^L)_{ijk}^n$, $\underline{E}_{ijk}^n$ and $\underline{H}_{ijk}^{n+\frac{1}{2}}$ which are calculated at previous time steps $t=n\Delta t$ and $t=(n+\frac{1}{2})\Delta t$:

$$(E_{ijk}^{n+1})_x = -(a_{0x} / a_1), \tag{2.30}$$

$$(E_{ijk}^{n+1})_y = -(a_{0y} / a_1), \tag{2.31}$$

$$(E_{ijk}^{n+1})_z = -(a_{0z} / a_1), \tag{2.32}$$

where a_{0x}, a_{0y}, a_{0z}, and a_1 are given by

$$a_{0x} \equiv \Big\{ \frac{\Delta t}{\Delta z} [(H_{ij(k+\frac{1}{2})}^{n+\frac{1}{2}})_y - (H_{ij(k-\frac{1}{2})}^{n+\frac{1}{2}})_y] - \frac{\Delta t}{\Delta y} [(H_{i(j+\frac{1}{2})k}^{n+\frac{1}{2}})_z - (H_{i(j-\frac{1}{2})k}^{n+\frac{1}{2}})_z] \Big\} + \frac{\Delta t}{2} (E_{ijk}^n)_x \sum_\kappa \sigma_\kappa^{(0)}$$

$$+ Re\Big\{ [(J_\kappa^L)_{ijk}^n]_x \sum_\kappa \frac{1}{\theta_\kappa^L} [1 - exp(-\theta_\kappa^L \Delta t)] \Big\} + (E_{ijk}^n)_x Re\Big\{ \sum_\kappa [(\xi_{\kappa,0}^L) - (\xi_{\kappa,1}^L)] \Big\}$$

$$- \epsilon_o \epsilon_\infty (E_{ijk}^n)_x + \epsilon_o Re\Big\{ [(Q_\rho^L)_{ijk}^n]_x \sum_\rho [exp(-\gamma_\rho^L \Delta t) - 1] \Big\} + \epsilon_o (E_{ijk}^n)_x Re\Big\{ \sum_\rho [(\psi_{\rho,0}^L) - (\psi_{\rho,1}^L)] \Big\}, \tag{2.33}$$

$$a_{0y} \equiv \Big\{ \frac{\Delta t}{\Delta x} [(H_{(i+\frac{1}{2})jk}^{n+\frac{1}{2}})_z - (H_{(i-\frac{1}{2})jk}^{n+\frac{1}{2}})_z] - \frac{\Delta t}{\Delta z} [(H_{ij(k+\frac{1}{2})}^{n+\frac{1}{2}})_x - (H_{ij(k-\frac{1}{2})}^{n+\frac{1}{2}})_x] \Big\} + \frac{\Delta t}{2} (E_{ijk}^n)_y \sum_\kappa \sigma_\kappa^{(0)}$$

$$+ Re\Big\{ [(J_\kappa^L)_{ijk}^n]_y \sum_\kappa \frac{1}{\theta_\kappa^L} [1 - exp(-\theta_\kappa^L \Delta t)] \Big\} + (E_{ijk}^n)_y Re\Big\{ \sum_\kappa [(\xi_{\kappa,0}^L) - (\xi_{\kappa,1}^L)] \Big\}$$

$$- \epsilon_o \epsilon_\infty (E_{ijk}^n)_y + \epsilon_o Re\Big\{ [(Q_\rho^L)_{ijk}^n]_y \sum_\rho [exp(-\gamma_\rho^L \Delta t) - 1] \Big\} + \epsilon_o (E_{ijk}^n)_y Re\Big\{ \sum_\rho [(\psi_{\rho,0}^L) - (\psi_{\rho,1}^L)] \Big\}, \tag{2.34}$$

$$a_{0z} \equiv \Big\{ \frac{\Delta t}{\Delta y} [(H_{i(j+\frac{1}{2})k}^{n+\frac{1}{2}})_x - (H_{i(j-\frac{1}{2})k}^{n+\frac{1}{2}})_x] - \frac{\Delta t}{\Delta x} [(H_{(i+\frac{1}{2})jk}^{n+\frac{1}{2}})_y - (H_{(i-\frac{1}{2})jk}^{n+\frac{1}{2}})_y] \Big\} + \frac{\Delta t}{2} (E_{ijk}^n)_z \sum_\kappa \sigma_\kappa^{(0)}$$

$$+ Re\Big\{ [(J_\kappa^L)_{ijk}^n]_z \sum_\kappa \frac{1}{\theta_\kappa^L} [1 - exp(-\theta_\kappa^L \Delta t)] \Big\} + (E_{ijk}^n)_z Re\Big\{ \sum_\kappa [(\xi_{\kappa,0}^L) - (\xi_{\kappa,1}^L)] \Big\}$$

$$- \epsilon_o \epsilon_\infty (E_{ijk}^n)_z + \epsilon_o Re\Big\{ [(Q_\rho^L)_{ijk}^n]_z \sum_\rho [exp(-\gamma_\rho^L \Delta t) - 1] \Big\} + \epsilon_o (E_{ijk}^n)_z Re\Big\{ \sum_\rho [(\psi_{\rho,0}^L) - (\psi_{\rho,1}^L)] \Big\}, \tag{2.35}$$

$$a_1 \equiv \epsilon_o \epsilon_\infty + \frac{\Delta t}{2} \sum_\kappa \sigma_\kappa^{(0)} + Re\Big\{ \sum_\kappa (\xi_{\kappa,1}^L) \Big\} + \epsilon_o Re\Big\{ \sum_\rho (\psi_{\rho,1}^L) \Big\}. \tag{2.36}$$

In our FDTD approach, we basically need to update Eqs. (2.7-2.9), (2.15), (2.27) and (2.30-2.32), respectively, for $\underline{H}_{ijk}^{n+\frac{1}{2}}$, $(Q_\rho^L)_{ijk}^{n+1}$, $(\underline{J}_\kappa^L)_{ijk}^n$ and $\underline{E}_{ijk}^{n+1}$ at each time step in order to carry out a complete three-dimensional computer simulation of the electric field response in linear dispersive materials that contain both frequency-dependent electric conductivity and polarization terms.

III.   SAMPLE FDTD CALCULATIONS: ONE-DIMENSIONAL CASE STUDY FOR THE PENETRATION OF MICROWAVES THROUGH CONCRETE

To understand dispersive effects in penetration through concrete, we first perform one-dimensional simulations of narrow-band, wide-band and ultrawide-band electromagnetic pulses penetrating through finite-thickness concrete using the newly formulated FDTD algorithm. We perform separate simulations for narrow-band, wide-band, and ultrawide-band incident electromagnetic pulses to investigate the effect of the pulse shape in the transmitted wave. For these simulations, we launch a time-dependent electromagnetic pulse in free-space at 8.46 cm (5 grid cells) from the left-hand edge of the computational space and propagate the pulse from left to right in the positive x-direction. After traveling 16.83 meters (995 grid cells), the pulse is first incident on 20.30 cm (12 grid cells) thick dispersive concrete that is characterized by first-order, time-dependent electric susceptibility and conductivity. After penetrating through dispersive concrete, the wave continues to propagate in free-space for another 16.71 meters (988

grid cells) until it reaches the right hand edge of the computational space that is terminated by a LIAO absorbing boundary condition [15]. Also, the LIAO absorbing boundary condition is used at the left-hand edge to absorb all reflected waves. To model the dispersive behavior of concrete at microwave frequencies, we consider the Debye forms for the first-order, time-dependent, electric susceptibility and conductivity functions [see Eqs. (1.3) and (1.4)] by expressing α_p^L, β_κ^L, γ_p^L, and θ_κ^L in terms of the following real constants:

$$\alpha_p^L = \delta(\epsilon_s - \epsilon_\infty) \quad \text{and} \quad \gamma_p^L = \delta , \tag{3.1}$$

$$\beta_\kappa^L = \varpi(\sigma_s - \sigma_\infty) \quad \text{and} \quad \theta_\kappa^L = \varpi , \tag{3.2}$$

where δ is the first-order electric susceptibility damping frequency, ϵ_s is relative permittivity at $\omega = 0$, ϵ_∞ is relative permittivity at $\omega = $ infinity, ϖ is the first-order conductivity damping frequency, σ_s is electrical conductivity at $\omega = 0$, and σ_∞ is electrical conductivity at $\omega = $ infinity. In our sample FDTD calculation, we treat the case where the dispersive properties of concrete are represented only by one first-order, time-dependent, electric susceptibility function and one first-order, time-dependent, conductivity function; namely, we set $\rho_{max} = 1$ and $\kappa_{max} = 1$ in our FDTD algorithm obtained in the previous section. Also, we set $\sigma_\kappa^{(0)}$ to be equal to σ_∞ so that the electrical conductivity contribution is properly taken into account at $\omega = 0$.

For our simulations, we investigate three different incident pulses: the sine-wave pulse (narrow-band), the frequency-band filtered sinc function pulse (wide-band), and the Gaussian pulse (ultrawide-band). We use the following mathematical expressions for launching of the three incident pulses:

- For the sine-wave pulse: *Incident Pulse(t) = A sin(ω_c t)[U(t) - U(t - t_{width})]* (3.3)

- For the frequency-band filtered sinc function pulse:

$$Incident\ Pulse(t) = A \{\ sinc\ [(\omega_a(t - t_{delay})] - \frac{\omega_b}{\omega_a} sinc\ [(\omega_b(t - t_{delay})]\ \}U(t), \tag{3.4}$$

- For the Gaussian pulse: $Incident\ Pulse(t) = A\ exp[\dfrac{(t - t_{delay})}{t_{width}}] U(t),$ (3.5)

where A is the amplitude of the electric field and t_{delay} is the delay time for the incident pulse. We arbitrarily assign A to have the value of 1.0 volt/meter, t_{width} to have values of 4.23×10^{-9} second (150 times that of the time increment) and 3.387×10^{-10} second (12 times that of the time increment), respectively, for the sine-wave pulse and the Gaussian pulse, t_{delay} to have the value of 2.82×10^{-8} second for both the frequency-band filtered sinc function pulse and the Gaussian pulse, and ω_a and ω_b to take values of 1.128×10^{10} radians/second and 4.512×10^{10} radians/second, respectively. Figure1, Figure 2 and Figure 3 show the time-domain and frequency-domain plots of the three incident waves we use in our simulations.

We select the total number of simulation cells to be 2000, ranging from $x = -1000$ to $x = 1000$, with the free-space/concrete interfaces located at $x = 0$ and x=8. We launch a pulse into free space 5 grid cells to the right of the left-hand edge (at $x = -1000$) and the pulse travels in the positive x-direction. We use the LIAO absorbing boundary condition [15] at both ends of the computational space.

Following are the basic FDTD parameters that we use in our one-dimensional simulations:

Uniform grid cell size (Δx) = 1.691 centimeters,

Total simulation distance (Δx times the total number of cells) = 33.82 meters,

Time step increment ($\Delta t = \Delta x / 2c$) = 28.2 picoseconds,

Total number of time steps = 5000 (total simulation time = 0.141 microsecond),

where c is the speed of light.

To assign values for parameters that describe the material properties of dispersive concrete as seen in Eqs. (3.1) and (3.2), we make use of the concrete data shown in Figures 4 and 5 [1], specifically selecting the curves at the saturation level (S) of 0.5.

$\epsilon_s = 5.5$; $\epsilon_\infty = 7.5$; and $\delta = 2.497 \times 10^{-9}$ second; $\sigma_s = 0.05$ mhos; $\sigma_\infty = 0.15$ mhos; $\varpi = 2.0 \times 10^{-10}$ second.

Results of the fully dispersive FDTD calculations are shown in Figure 6, Figure 7 and Figure 8, respectively, for the sine-wave pulse, the frequency-band filtered sinc function pulse, and the Gaussian pulse. These figures are snap shots of the spatial electric field patterns taken at time steps of 1,500 and 3,500 (i.e., before and after the wave penetrates through concrete).

To compare results of our fully dispersive FDTD calculations with non-dispersive FDTD calculations, we perform nondispersive FDTD calculations using the average permittivity and conductivity values centered on the middle frequency of the incident pulse. Shown in Figure 9, Figure 10 and Figure 11 are the relative cumulative energy of the pulses that penetrate through concrete, respectively, for the sine-wave pulse, the frequency-band filtered sinc function pulse, and the Gaussian pulse. From these figures we can see that the wider the incident pulse the greater the discrepancy between fully dispersive and non-dispersive FDTD calculations. It clearly indicates the importance of carrying out the fully dispersive FDTD calculations for dispersive concrete if the incident pulse is considered to be relatively broad over the frequency range where the permittivity and conductivity values change significantly.

IV. CONCLUSIONS

Based on the FDTD approach we presented here, we can solve three-dimensional Maxwell's equations directly for the propagation of electromagnetic waves in linear dispersive materials that exhibit both frequency-dependent electrical conductivity and polarization. Because of the piecewise linear approximation we used for the time dependent part of the electric field vector, our approach provides second order accuracy in time. In addition, our approach retains all the advantages of the usual first-order discrete recursive convolution approach, such as fast computational speed and efficient use of computer memory.

We have shown that it is critical to express the first-order, time-dependent electric susceptibility and conductivity functions in the exponential forms in order to obtain the recursive relationships in our FDTD algorithm. An important result we have shown in this paper is that our FDTD algorithm provides second order accuracy in both time and space.

Our sample one-dimensional FDTD calculations show that it is very important to include fully dispersive effects in the analysis of microwaves penetration through concrete, especially for wide-band and ultrawide-band incident pulses, because concrete shows significant frequency-dependent conductivity and permittivity at microwave frequencies. Use of the simple frequency-averaged conductivity value in a nondispersive FDTD calculation will not result in predicting the correct amount of wave energy that penetrates through concrete.

REFERENCES:

[1] C. Courtney, J. Lehr, D. Mason, B. Motil and A. Lovesee, "Measurement and Characterization of the Electromagnetic Properties of Materials," Voss Scientific Document No. VS-603, Aug 1996

[2] C. J. Myers and D. E. Voss, "Material Modeling Approach for the Study of Microwave Propagation in Concrete," Voss Scientific Document No. VS-701, Aug 1997

[3] J. Rohrbaugh, "Shielding Effectiveness of Concrete: Literature Search Results," US Air Force's Phillips Laboratory/WST Internal Report, Kirtland AFB, NM, Draft2, 10 Oct 1995

[4] K. S. Yee, "Numerical Solution of Initial Boundary Value Problems Involving Maxwell's Equations in Isotropic Media," IEEE Trans. Antenna Propagat., vol AP-14, pp. 302-307, 1966

[5] R. J. Luebbers, F. Hunsberger and K. S. Kunz, "A Frequency-dependent Finite Difference Time-Domain Formulation for Transient Propagation in Plasma," IEEE Trans. Antennas and Propagat., vol 39, pp. 29-34, 1991

[6] R. M. Joseph, S. C. Hagness and A. Taflove, "Direct Time Integration of Maxwell's Equations in Linear Dispersive Media with Absorption for Scattering and Propagation of Femtosecond Electromagnetic Pulses," Opt. Lett., vol 16, 1412-1414, 1991

[7] R. J. Luebbers and F. Hunsberger, "FDTD for Nth-order Dispersive Media," IEEE Trans. Antenna and Propagat., vol 40, pp. 1297-1301, 1992

[8] F. Hunsberger, R. Luebbers and K. Kunz, "Finite-Difference Time-Domain Analysis of Gyrotropic Media-I: Magnetic Plasma," IEEE Trans. Antennas and Propagat., vol 40, pp. 1489-1495, 1992

[9] R. Luebbers, D. Steich and K. Kunz, "FDTD Calculation of Scattering from Frequency-dependent Materials," IEEE Trans. Antennas and Propagat., pp. 1249-1257, 1993

[10] J. L. Young, "Propagation in Linear Dispersive Media: Finite Difference Time-Domain Methodologies," IEEE Trans. Antennas and Propagat., vol 43, pp. 411-430, 1995

[11] A. Taflove, *Computational Electromagnetics: The Finite-Difference Time-Domain Method*, Boston: Artech House, 1995

[12] S. J. Yakura and J. MacGillivray, "Finite-Difference Time-Domain Calculations Based on the Recursive Convolution Approach for Propagation of Electromagnetic Waves in Nonlinear Dispersive Media," Air Force Research Laboratory Report (PL-TR-97-1170) – Appendix, Oct 30, 1997.

[13] D. F. Kelley and R. J. Luebbers, "Piecewise Linear Recursive Convolution for Dispersive Media Using FDTD," IEEE Trans. Antenna and Propagat., vol 44, pp. 792-797, 1996

[14] S. J. Yakura, J. T. MacGillivray and D. Dietz "A Finite-Difference Time-Domain Algorithm Based on the Recursive Convolution Approach for Propagation of Electromagnetic Waves in Nonlinear Dispersive Media," The 15th Annual Review of Progress in Applied Computational Electromagnetics, vol 1, pp. 4-11, ACES Meeting, Monterey, CA., Mar 1999

[15] Z. P. Liao, H. L. Wong, B. P. Yang and Y. F. Yuan, "A Transmitting Boundary for Transient Wave Analysis," Scientia Sinica, vol XXVII, pp. 1063-1076, 1984
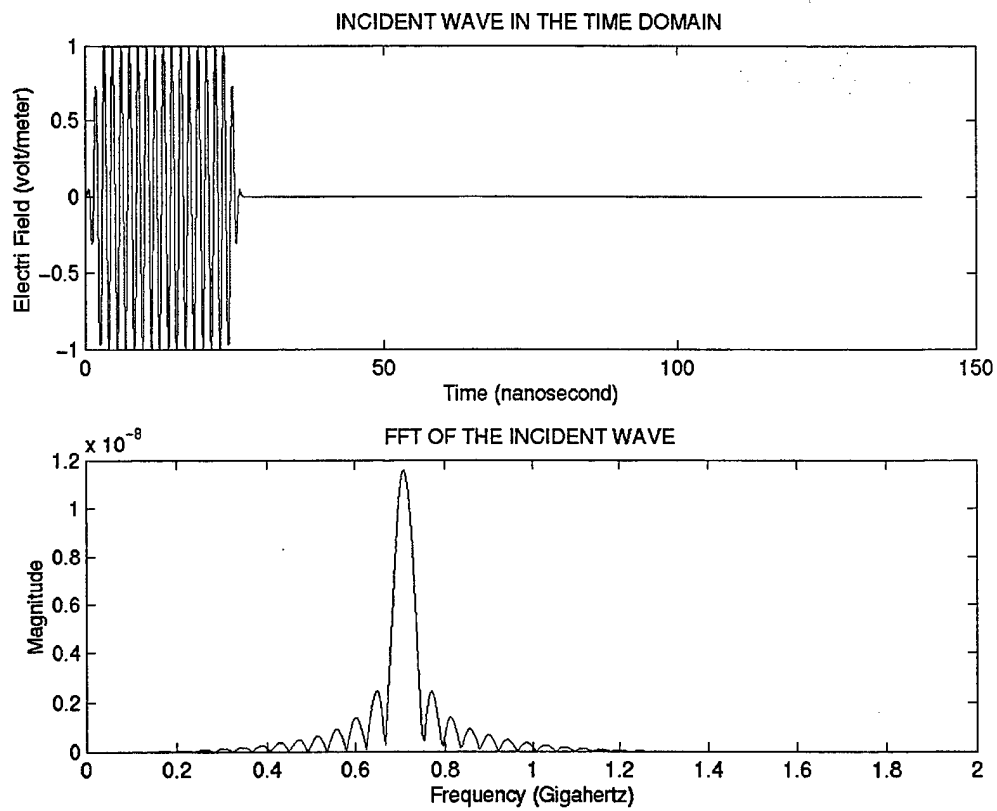
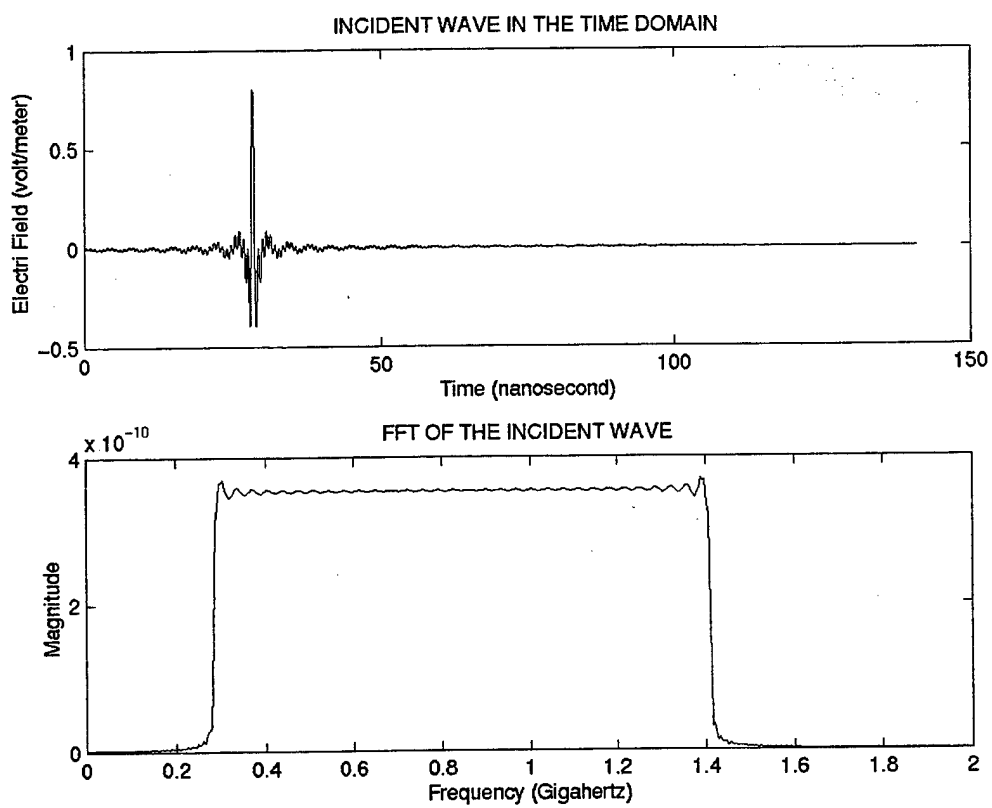Figure 1: Time-domain (top figure) and frequency-domain (bottom figure) plots of a sine-wave incident pulse.

Figure 2: Time-domain (top figure) and frequency-domain (bottom figure) plots of a frequency-band filtered sinc function incident pulse.
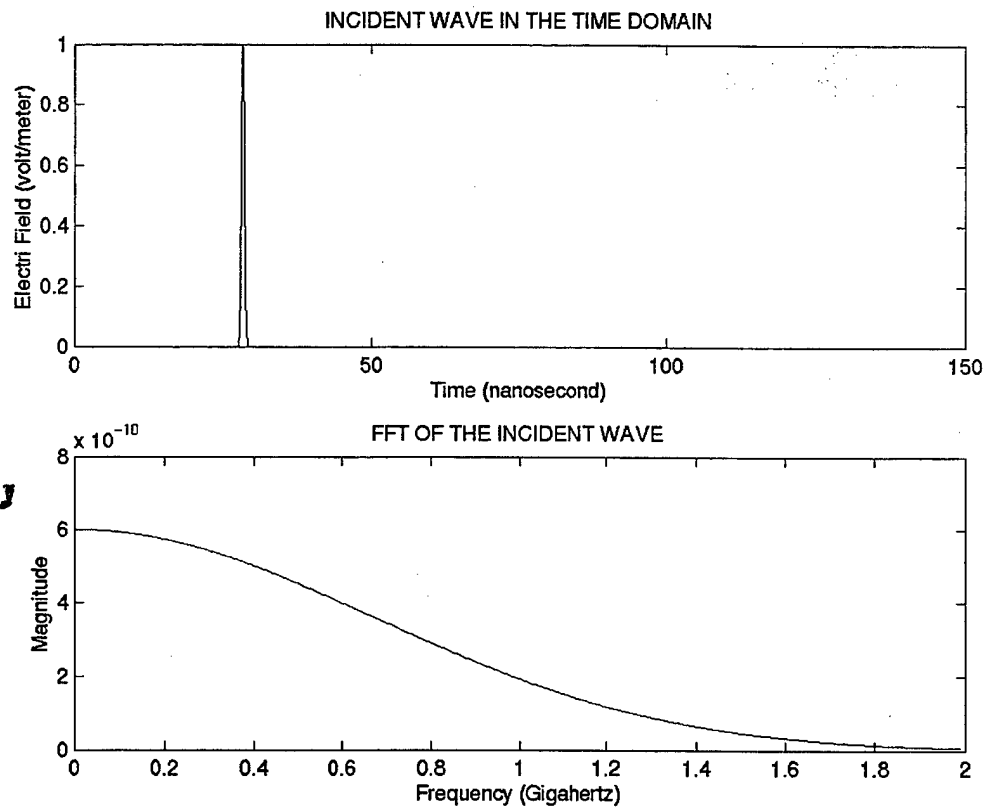
Figure 3: Time-domain (top figure) and frequency-domain (bottom figure) plots of a Gaussian incident pulse.
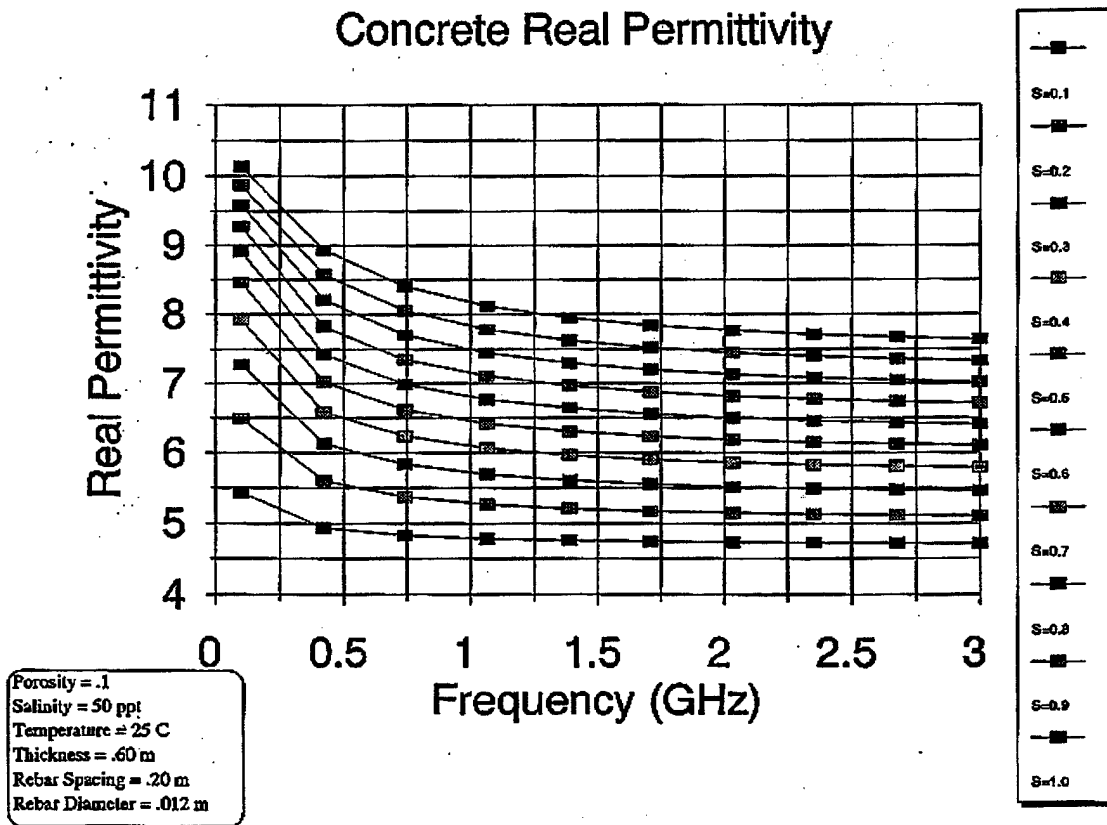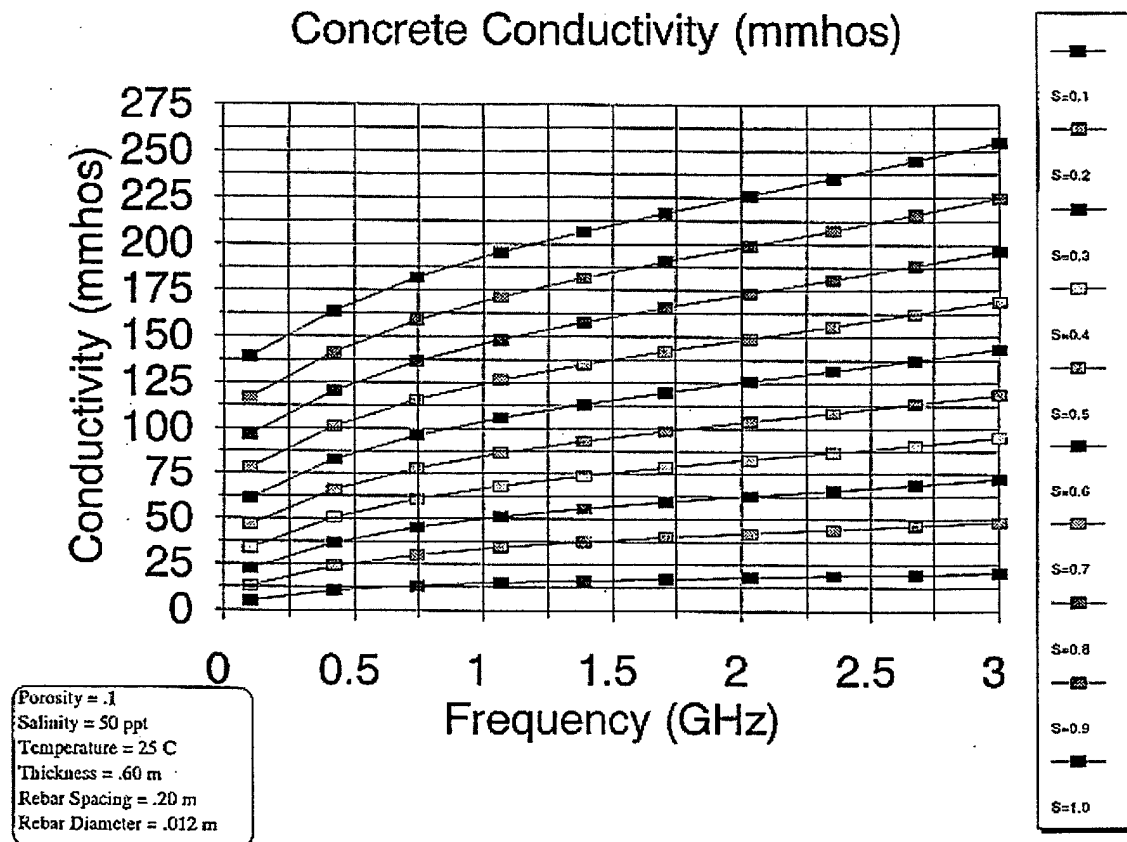
Figure 4: Concrete Permittivity Data [Reference 1]

(note: The legend in the left-hand side shows the specific condition that the data is evaluated for. Also, the legend in the right-hand side is for the saturation level with saturation levels (S) ranging from 0.1 (10%) to 1.0 (100%) in the increment of 0.1)
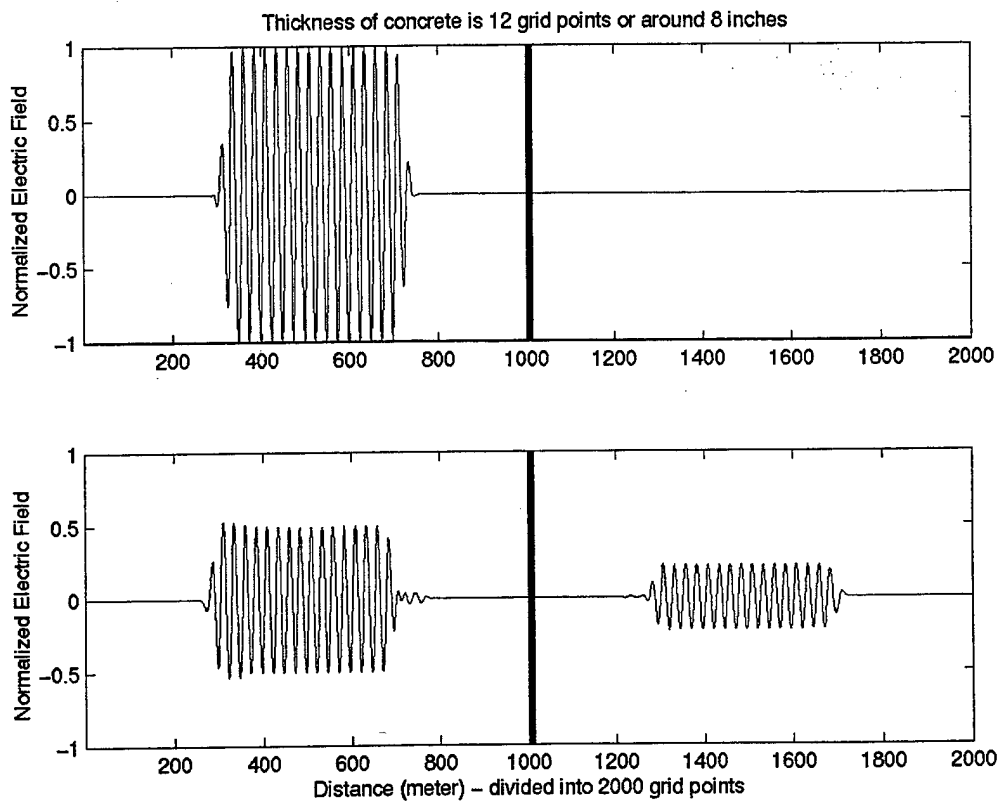
Figure 5: Concrete Conductivity Data [Reference 1]

(note: The legend in the left-hand side shows the specific condition that the data is evaluated for. Also, the legend in the right-hand side is for the saturation level with saturation levels (S) ranging from 0.1 (10%) to 1.0 (100%) in the increment of 0.1)

Thickness of concrete is 12 grid points or around 8 inches

Figure 6: Spatial electric field profiles for a sine-wave pulse taken at time steps = 1,500 (top figure) and
3,500 (bottom figure). A bold line in the middle represents the thickness of concrete
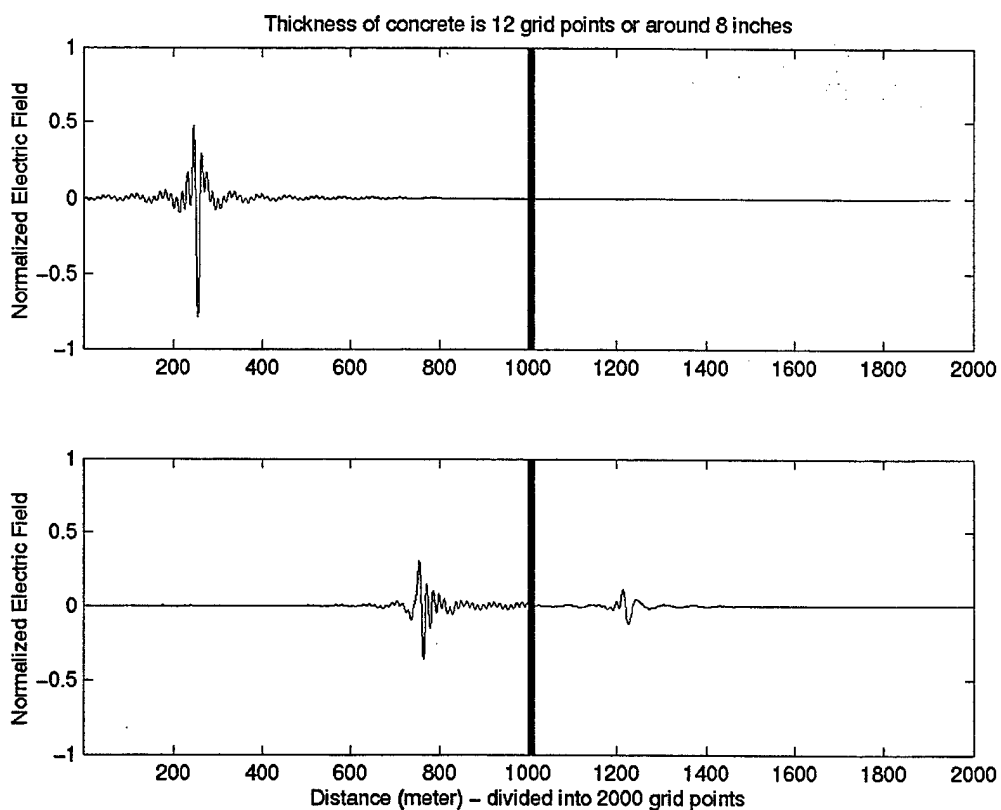(12 grid cells or 8 inches).

Figure 7: Spatial electric field profiles for a frequency-band filtered sinc function pulse taken at time steps = 1,500 (top figure) and 3,500 (bottom figure). A bold line in the middle represents the thickness of concrete (12 grid cells or 8 inches).
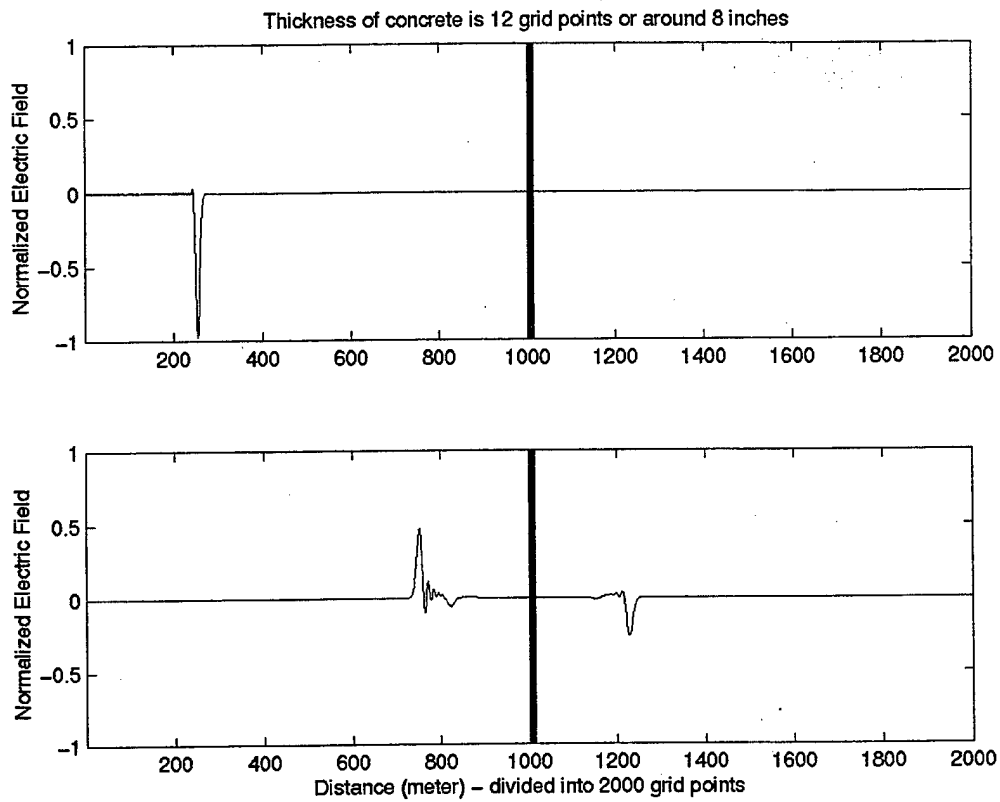
Figure 8: Spatial electric field profiles for a Gaussian pulse taken at time steps = 1,500 (top figure) and 3,500 (bottom figure). A bold line in the middle represents the thickness of concrete (12 grid cells or 8 inches).

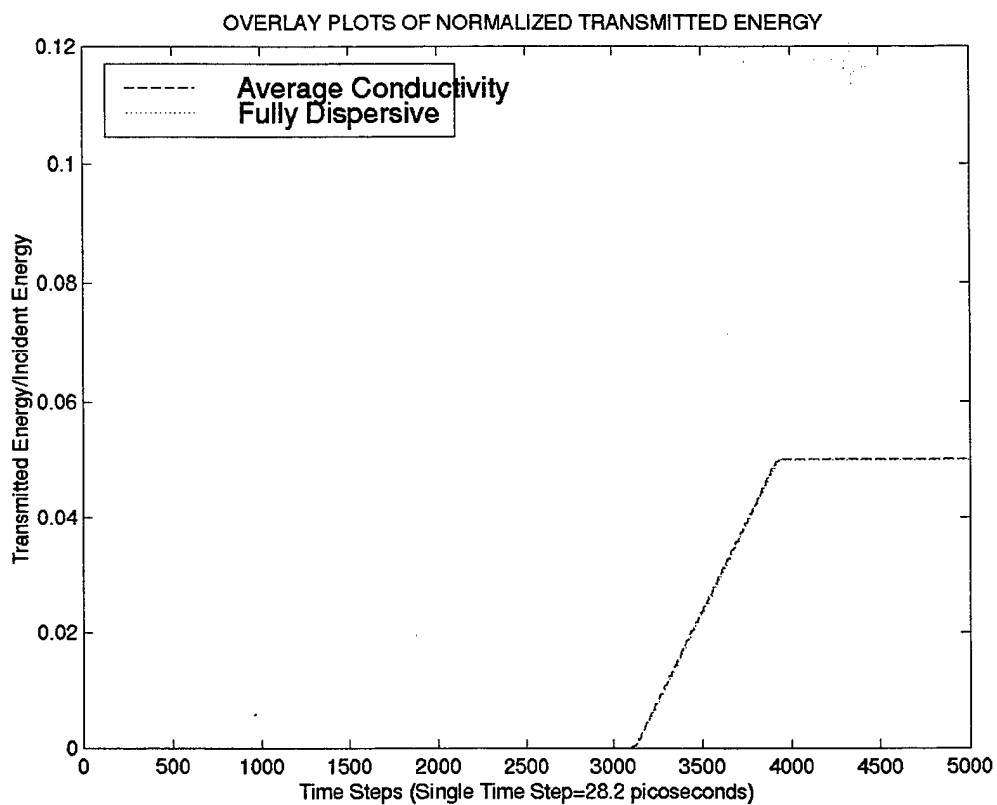OVERLAY PLOTS OF NORMALIZED TRANSMITTED ENERGY

Figure 9: Overlay plots of cumulative power penetrated through concrete for fully dispersive FDTD and nondispersive (with the average conductivity value) FDTD calculations in the case of a sine-wave pulse.

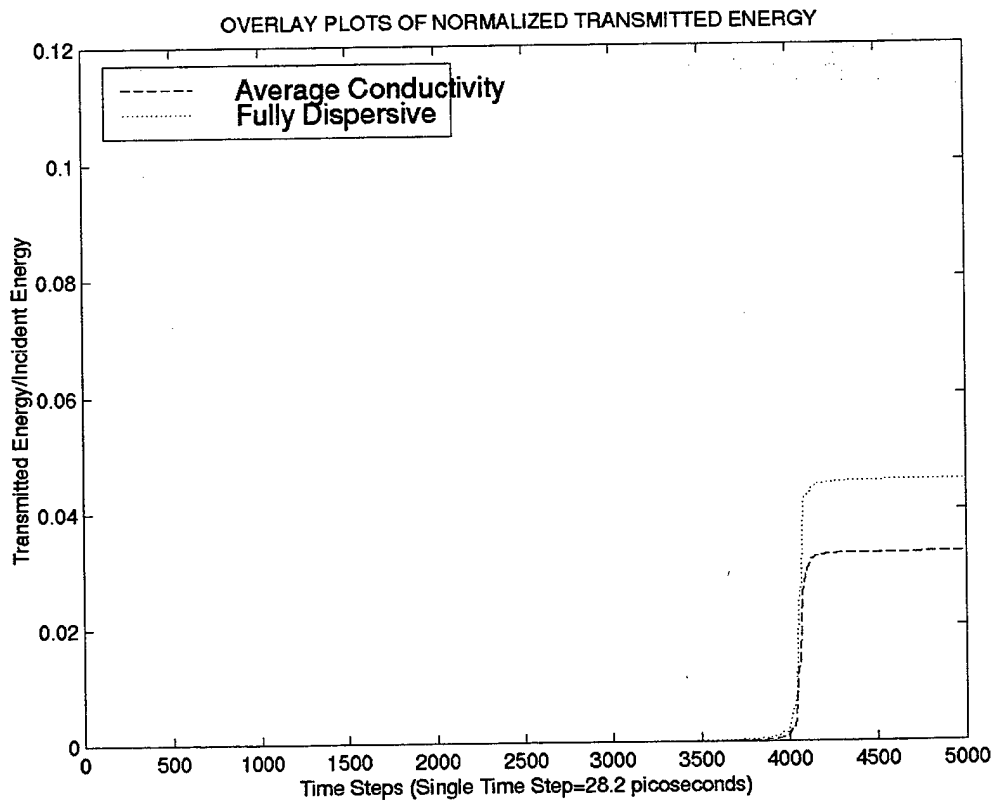OVERLAY PLOTS OF NORMALIZED TRANSMITTED ENERGY

Figure 10: Overlay plots of cumulative power penetrated through concrete for fully dispersive FDTD and nondispersive (with the average conductivity value) FDTD calculations in the case of a frequency-band filtered sinc function pulse.
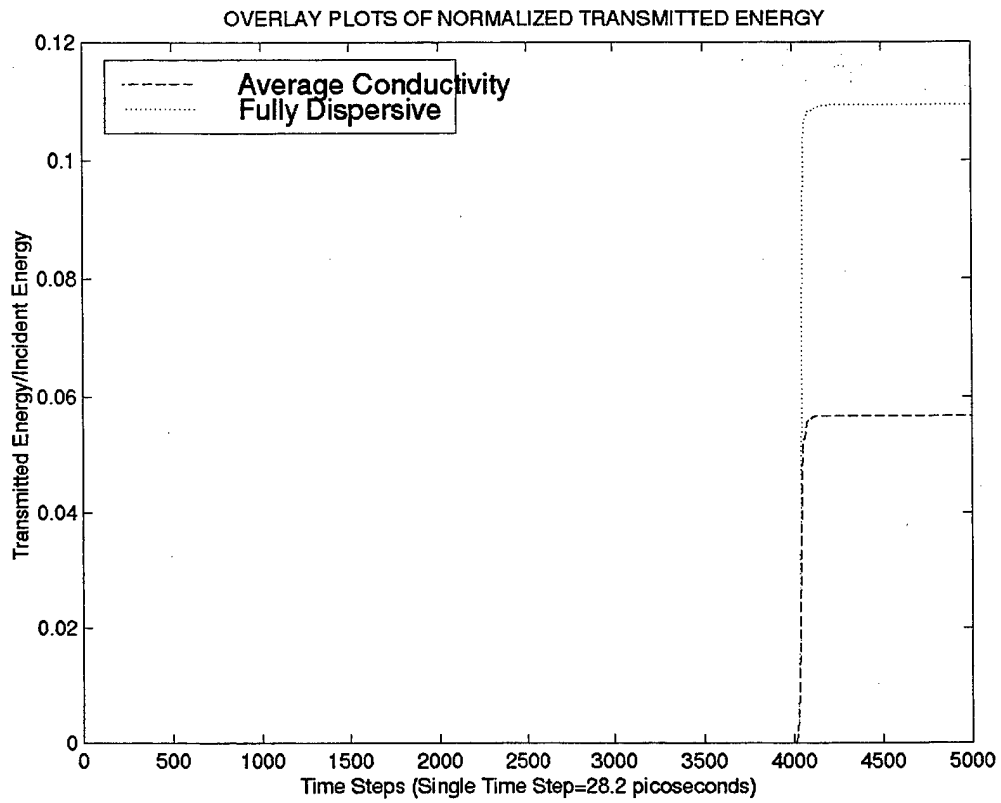
OVERLAY PLOTS OF NORMALIZED TRANSMITTED ENERGY

Figure 11: Overlay plots of cumulative power penetrated through concrete for fully dispersive FDTD and nondispersive (with the average conductivity value) FDTD calculations in the case of a Gaussian pulse.

DISTRIBUTION LIST

AUL/LSE
Bldg 1405 - 600 Chennault Circle
Maxwell AFB, AL 36112-6424   1 cy

DTIC/OCP
8725 John J. Kingman Rd, Suite 0944
Ft Belvoir, VA 22060-6218   2 cys

AFSAA/SAI
1580 Air Force Pentagon
Washington, DC 20330-1580   1 cy

AFRL/PSTL
Kirtland AFB, NM 87117-5776   2 cys

AFRL/PSTP
Kirtland AFB, NM 87117-5776   1 cy

AFRL/DE/Dr Hogge
Kirtland AFB, NM 87117-5776   1 cy

Official Record Copy
AFRL/DEPE/Dr Dietz
Kirtland AFB, NM 87117-5776   5 cy

Official Record Copy
AFRL/DEPE/Dr Yakura
Kirtland AFB, NM 87117-5776   5 cys